Upconversion Nanoparticles

International Edition: DOI: 10.1002/anie.201906380
German Edition: DOI: 10.1002/ange.201906380

Boosting Luminance Energy Transfer Efficiency in Upconversion Nanoparticles with an Energy-Concentrating Zone

Xiaobo Zhang[+], Weiwei Chen[+], Xiaoyu Xie[+], Yuyi Li, Desheng Chen, Zhicong Chao, Chenghui Liu, Haibo Ma, Ying Liu, and Huangxian Ju**

Abstract: *Despite the successful application of upconversion nanoparticles (UCNPs), their low energy transfer efficiency is still a bottleneck to further applications. Here we design UCNPs with a multilayer structure, including an inert $NaYF_4$:Gd core and an energy-concentrating zone (ECZ), for efficient energy concentration. The ECZ is composed of an emitting layer of $NaYF_4$:Yb,Er and an absorption layer of $NaYF_4$:Nd,Yb with antenna IRDye 800CW to manipulate the energy transfer. The stable and tight packing of 800CW linked originally with a bisphosphonate ligand improves greatly the transfer efficiency. The proximity of the emitting layer to both surface antenna and accepter also decreases energy depletion. Compared to classical UCNPs, the ECZ UCNPs show 3600 times higher luminescence intensity with an energy transfer efficiency near 60 %. In proof-of-concept applications, this type of structure was employed for Hg^{2+} detection and for photodynamic therapy under hypoxic conditions.*

Photon upconversion indicates a process of absorbing low-energy near-infrared (NIR) photons to emit higher energy photons.[1] This process can be performed with upconversion nanoparticles (UCNPs), a class of nanomaterials doped with lanthanide ions,[2] which provides a large anti-Stokes shift with sharp emission to act as favorable energy donors in luminescence resonance energy transfer (LRET).[3] Although the LRET of UCNPs has been extensively applied in biosensing and biomedicine, the low energy transfer efficiency due to the relatively low extinction coefficients of lanthanide dopants[4] and the constraint in nanoparticle dimension[5] of UCNPs is still a bottleneck to further applications.

Several multilayer UCNPs have been proposed to enhance the transfer efficiency.[6–10] However, assembling a spacer layer[7] or an inert shell[8] on UCNPs increases the distance from the emitter to the surface LRET acceptor, while some approaches to reduce particle size[9] increase surface quenching and lower the quantum yield.[1b] To overcome the distance effect, a thin shell of $NaYbF_4$:Tm has been constructed on UCNPs for confining energy in the shell to enhance the upconversion luminescence.[10] Unfortunately the total luminescence intensity of UCNPs is still limited due to the low light absorption capability of rare-earth elements. Hence, some NIR dyes with large optical cross-section have been attached to UCNPs as antenna for improving the light absorption.[11] The modification is generally performed with poly(acrylic acid), polyethyleneimine (PEI), or silica coating as the surface linker,[11e–g] which extends energy transfer distance again, and thus causes energy depletion during migration.[12]

To boost efficiently the energy transfer efficiency in UCNPs, we propose herein the new concept of an energy-concentrating zone (ECZ) and report on an energy concentration mechanism in which an inert core is used to confine energy in a thin layer close to UCNPs surface and a bisphosphonate ligand is used to link IRDye 800CW as the light-absorbing antenna on the surface. The ECZ includes an energy-emitting layer $NaYF_4$:Yb,Er and an energy absorption layer $NaYF_4$:Nd,Yb with antenna 800CW attached to its surface with alendronic acid (ADA) (Figure 1). The high binding energy between lanthanide ions and bidentate phosphate guarantees the stable and tight packing of antenna for energy adsorption and inward transfer. The inert core

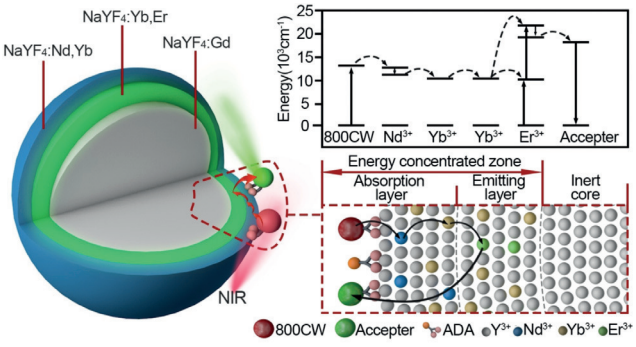

Figure 1. UCNPs structured with an energy-concentrating zone to boost energy transfer efficiency and a simplified energy level diagram.

[*] X. B. Zhang,[+] W. W. Chen,[+] Y. Y. Li, Z. C. Chao, Prof. Y. Liu, Prof. H. X. Ju
State Key Laboratory of Analytical Chemistry for Life Science
School of Chemistry and Chemical Engineering
Nanjing University
Nanjing 210023 (China)
E-mail: yingliu@nju.edu.cn
hxju@nju.edu.cn
X. Y. Xie,[+] Prof. H. B. Ma
Institute of Theoretical and Computational Chemistry Department
School of Chemistry and Chemical Engineering
Nanjing University
Nanjing 210023 (China)
D. S. Chen, Prof. C. H. Liu
School of Chemistry and Chemical Engineering
Shaanxi Normal University, Xi'an 710062 (China)
[+] These authors contributed equally to this work.
Supporting information and the ORCID identification number(s) for the author(s) of this article can be found under: https://doi.org/10.1002/anie.201906380.

blocks the energy transfer to deep interior of UCNPs and spatially concentrates it in proximity to UCNP surface, thus enhancing the local density of excitation energy, and boosting the LRET efficiency by decreasing the distance of energy transfer outward to the surface-attached acceptor. Thus, the energy concentration efficiently enhances the LRET efficiency up to 60% and produces a luminescence intensity 3600 times higher than that of classical UCNPs. By conjugating the fluorescence dye or photosensitizer as the functional acceptor to UCNPs, the ECZ UCNPs successfully demonstrate the improved sensitivity for analytical applications and high yield to produce reactive oxygen species (ROS) for photodynamic therapy (PDT) in hypoxic environment. The proposed concept and strategy provides a versatile platform for probing the upconversion mechanism and LRET-based applications.

$NaYF_4$:Yb,Er@$NaYF_4$:Nd,Yb (UCNP1, 30.4 nm) was synthesized by coating a $NaYF_4$:Nd,Yb shell on a $NaYF_4$:Yb,Er core (20.0 nm) (Figure 2A and Figure S1A). The shell–core structure demonstrated a characteristic absorption peak at 800 nm that well overlapped with the emission peak of IRDye 800CW to facilitate light harvest (Figure 2B),[13] at which the UCNPs showed strong emission peaks at 520, 542, and 660 nm due to the large cross section of Nd^{3+} (Figure S1B). UCNP-ADA showed the characteristic peak of P=O at 1013 cm^{-1} (Figure 2C, spectrum 2) and increased zeta potential and hydrodynamic diameter (Figure 2D). The fluorescence spectra of UCNP1-ADA-Cy3, UCNP1-AEP-Cy3, which was prepared with *o*-phosphorylethanolamine (AEP), and UCNP1-Cy3 demonstrated the surface-binding stability of ADA. Both UCNP-ADA-Cy3 and UCNP-AEP-Cy3 showed much higher fluorescence intensity than UCNP-Cy3, while the intensity of UCNP-ADA-Cy3 did not change and was more stable than UCNP-AEP-Cy3 and UCNP-Cy3 upon incubation in phosphate-buffered saline (PBS) for 60 min. Phosphate groups in PBS could replace AEP and carboxyl-group-derived Cy3 on the UCNP surface, which led to the fluorescence decrease of Cy3 upon incubation and removal of released Cy3 (Figure 2E,F). The stability of UCNP-ADA in cytoplasm was demonstrated by transfecting human cervix carcinoma (HeLa) cells with UCNP1-ADA-Cy3 or UCNP1-AEP-Cy3 (Figure S2A). Density functional theory (DFT) calculations further confirmed the stability of UCNP1-ADA (Figure S2B). ADA possesses larger binding energies for both facets of $NaYF_4$ than those of AEP and CH_3COO^- (Table S1), which was consistent with the trends in binding energies for carboxylic acid and phosphate groups reported previously.[14]

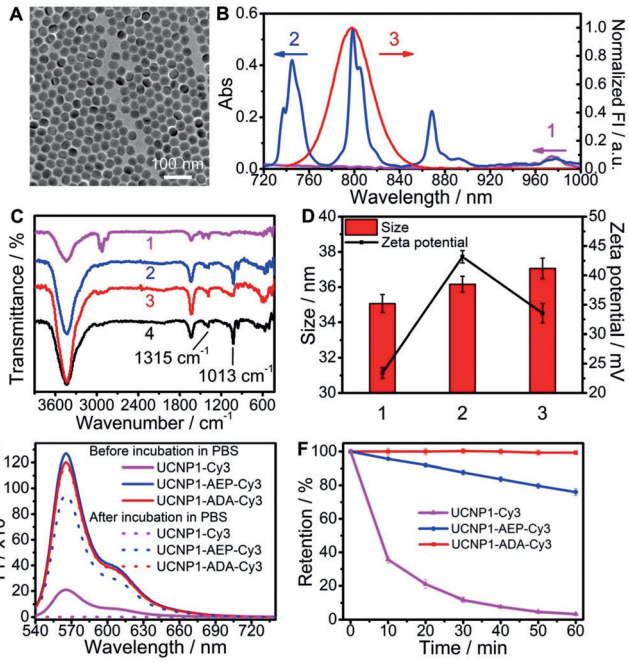

Figure 2. A) Transmission electron microscopic image of UCNP1. B) Absorption spectra of $NaYF_4$:Yb,Er core (1) and UCNP1 (2), and normalized emission spectrum of 800CW under 720 nm excitation (3). C) FTIR spectra of UCNP1 (1), UCNP1-ADA (2), 800CW (3) and UCNP1-ADA-800CW (4). D) Particle sizes and zeta potentials of bare UCNP1 (1), UCNP1-ADA (2), and UCNP1-ADA-800CW (3). E) Fluorescence spectra of 1 mg mL^{-1} UCNP1-ADA-Cy3, UCNP1-AEP-Cy3, and UCNP1-Cy3 after incubation in PBS for 1 h under 530 nm excitation and removal of the released Cy3 by centrifugation. F) Fluorescence retention percentages at 570 nm upon incubation in PBS for different times.

The antenna molecule 800CW possesses about 30000 times larger absorption cross section than Nd^{3+},[15] and its emission from 750 to 860 nm can well overlap with the main absorption peak of UCNP1 (Figure 2B and Figure S1C). The tight attachment of 800CW to UCNP1-ADA was characterized by an aromatic ether vibration at 1315 cm^{-1} and a slightly increased hydrodynamic diameter (Figure 2C,D). Compared with UCNP-800CW, UCNP1-ADA-800CW prepared with the same reaction ratio of 800CW to UCNPs (500:1) showed much stronger 800CW fluorescence (Figure S1D), indicating the higher loading capacity of 800CW on UCNP1-ADA. Moreover, in the absorption spectrum of UCNP1-ADA-800CW (Figure S1E) the maximum absorption peak is similar to 800CW (Figure S1C), indicating the impressive absorption capability of antennae-dye-modified UCNPs around 800 nm.

To demonstrate the ADA-facilitated energy transfer, UCNP1@SiO_2-NH_2 and UCNP1@PEI were prepared as controls (Figure S3A,B). For both, the amount of 800CW bound on the nanoparticles was determined to be 330 molecules per nanoparticle (Figure S3C–E). The 800CW wrapped in thick layer showed much lower fluorescence intensity due to the depletion of absorption energy during the inward migration process (Figure S4A,B). The energy transfer efficiency η from 800CW to Nd^{3+} could be estimated according to Equation (1).

$$\eta = 1 - \frac{\tau_2}{\tau_1} \quad (1)$$

Here τ_1 is the fluorescence lifetime of 800CW attached to $NaYF_4$:Yb,Er@$NaYF_4$:Yb (UCNP2) (Figure S4C), and τ_2 is the fluorescence lifetime of 800CW on UCNP1 with a different modification. The lifetime of 800CW on UCNP1-ADA was 303 ps, which was obviously shorter than that for UCNP2-ADA-800CW (1604 ps), UCNP1@SiO_2-800CW (1557 ps), and UCNP1@PEI-800CW (1375 ps) (Figure S4D). The transfer efficiency in UCNP1-ADA-800CW was 81.1%, impres-

sively higher than that of 14.2% for UCNP1@PEI-800CW and 2.9% for UCNP1@SiO_2-800CW. This can be explained by the tight packing of 800CW antenna via the ADA ligand.

The thickness of the absorption layer was an important parameter affecting the transfer efficiency and was optimized to be 2.7 nm (Figure S5). The energy transfer efficiency for UCNP1-ADA-800CW increased with the increasing thickness of the absorption layer, and trended to a stable value after a thickness of 2.7 nm, indicating the accumulation of Nd^{3+} and Yb^{3+} in the absorption layer benefited the inward transfer of absorbed energy. It should be pointed out that the thicker absorption layer did not obviously decrease the transfer efficiency, indicating the negligible energy depletion in the absorption layer. At an absorption layer thickness of 2.7 nm, the size of $NaYF_4$:Yb,Er core was optimized to be 24 nm (Figure S6), which led to a total size of UCNP1-ADA-800CW of 29.4 nm. When the total size increased from 26.7 to 57.4 nm, fluorescence intensity reached a maximum value at 29.4 nm and then continuously decreased by about threefold. This decrease could be attributed to the increased distance for energy migration through the crystal lattice, which usually leads to a depletion of the excitation energy for inward transfer.[16] Therefore, decreasing energy migration distance from emitter Er^{3+} to the UCNP surface could concentrate the emission and prompt its outward transfer, and ultimately enhance LRET efficiency.

To confine emitter Er^{3+} close to the UCNP surface to shorten the distance for emission energy outward transfer, multilayer UCNPs was synthesized with an inert core $NaYF_4$:Gd and an ECZ layer. The size of $NaYF_4$:Gd core was 20.6 nm, and the ECZ thickness was set at 5 nm considering the high resonance energy transfer efficiency for UCNPs,[5a,17] including the 2.3 nm emitting layer and the 2.7 nm absorption layer (Figure S7A). Compared with UCNP1-ADA-800CW (CS UCNPs), the 800CW-functionalized $NaYF_4$:Gd@$NaYF_4$:Yb,Er@$NaYF_4$:Nd,Yb (ECZ UCNP3-ADA-800CW or ECZ UCNPs) enhanced the luminance by twofold at the same size (Figure S7B), which was 3600 times stronger than that of UCNP1-ADA (Figure 3A). Similarly, the luminance enhancement was also observed from the photograph of 10 mg mL^{-1} UCNP3-ADA and 0.01 mg mL^{-1} ECZ UCNPs (Figure 3A).

The upconversion quantum yields of CS UCNPs and ECZ UCNPs under 808 nm excitation (1.5 W cm^{-2}) were further calculated according to a previous method[7] to be 2.48% and 3.33%, respectively, demonstrating the obvious improvement of energy utilization efficiency. Moreover, ECZ UCNPs could retain the brightness of 56.6% even with 808-nm irradiation at 1.5 W cm^{-2} for up to 5 h (Figure S8).

Generally, the energy transfer efficiency from donor to acceptor is distance dependent. Thus the excitation energy accepted by the surface accepter from different donors in the emitting layer is spatially inhomogeneous.[5a] A kinetic Monte Carlo model was established to indicate the energy distribution in the crystal structure of UCNPs (Figure S9A), and the emission photon counts corresponding to the distance to the UCNP surface (Figure 3B). All emission photons located within a 5 nm zone close to the surface for ECZ UCNPs, while only about 43% of the emission photons located in this zone

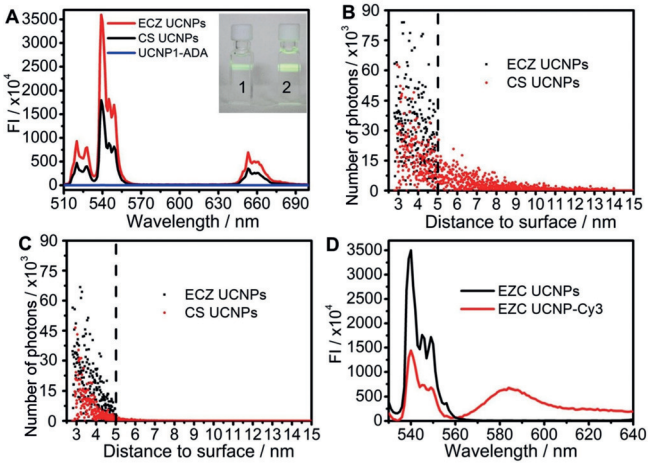

Figure 3. A) Upconversion emission spectra of 1 mg mL^{-1} ECZ UCNPs, CS UCNPs, and UCNP1-ADA under 808 nm excitation (10 W cm^{-2}). Inset: Luminance photographs of 10 mg mL^{-1} UCNP1-ADA (1) and 0.01 mg mL^{-1} ECZ UCNPs under the same excitation (2). B) Theoretical photon count emitted at different distances to the nanoparticle surface for ECZ UCNPs and CS UCNPs. C) Theoretical photon count absorbed from different distances to the nanoparticle surface for ECZ UCNPs and CS UCNPs. D) Emission spectra of 1 mg mL^{-1} ECZ UCNPs before and after Cy3 conjugation under 808 nm excitation (10 W cm^{-2}).

for CS UCNPs. The energy transfer efficiency η in LRET process was calculated according to Equation (2).

$$\eta = \frac{R_0^6}{R_0^6 + r^6} \tag{2}$$

Here R_0 denotes the Förster distance of the donor–acceptor pair, and r is the distance between donor Er^{3+} and the acceptor on the surface. Generally, the R_0 of the UCNP–dye pair is around 4 nm.[5a,17] Hence, the number of photons transferred to the surface accepter could be calculated by multiplying the energy transfer efficiency at a certain distance (Figure 3C), which showed that less than 20% of the emission photons were transferred to the surface receptor for the CS UCNPs, while the ratio increased to 60% for the ECZ UCNPs. Considering the good overlap of Cy3 at 552 nm with the emission spectrum of the ECZ UCNPs (Figure S9B), Cy3 was covalently conjugated to the ECZ UCNPs to verify the theoretical LRET efficiency. ECZ UCNP-Cy3 showed a strong emission peak at 585 nm with an obvious decrease of the emission peak from the ECZ UCNP at 542 nm (Figure 3D), indicating the efficient LRET process, while the same emission peak was hardly observed from CS UCNP-Cy3 (Figure S9C). The energy transfer efficiency of 59.02% calculated by lifetime detection for ECZ UCNPs was much greater than those of 10.18% for CS UCNPs and 30% for UCNPs with the same total size reported previously (Figure S9D),[6b,7,17] confirming the efficient energy migration in the ECZ layer. We further used a thin layer of Yb to avoid back energy transfer[7] and examined the performance of $NaYF_4$:Gd@$NaYF_4$:Yb,Er @$NaYF_4$:Yb@$NaYF_4$:Nd,Yb (UCNP4). In comparison with ECZ UCNPs, UCNP4-800CW demonstrated sixfold enhancement of UCNPs lumi-

nance at 540 nm, indicating the increased upconversion efficiency, while the energy transfer efficiency from Er^{3+} to surface Cy3 significantly decreased at 590 nm due to the increased distance (Figure S10), which is unfavorable for practical application.

With efficient concentration in energy absorption and emission, the ECZ UCNPs could greatly benefit LRET-based detection. Using Hg^{2+} as a model target, the dye N719 with a wide absorption centered at 535 nm (Figure 4A) was selected as the energy acceptor,[18] which obviously suppressed the emission of UCNPs. The optimal amount of N719 on ECZ UCNPs was 210 molecules per nanoparticle, at which N719 decreased the UC emission by 80.34% (Figure S11A). In the presence of Hg^{2+}, the maximum adsorption peak of N719 shifted significantly to 485 nm due to the binding of Hg^{2+}, which blocked the energy transfer from the emitting layer to N719, and led to the recovery of UCNPs emission (Figure 4B). The luminescence intensity at 540 nm linearly recovered with an increase in the Hg^{2+} concentration from 2 to 150 pM with a detection limit of 1.21 pM, which was 3 orders of magnitude lower than previous Hg^{2+} detection based on UCNPs (Figure 4C,D and Figure S11B).[18] The exciting improvement in sensitivity obviously resulted from the enhanced luminance intensity and energy transfer efficiency of ECZ UCNPs. Moreover, this method showed good selectivity, and other cations showed negligible response even at 6×10^7 times concentration (Figure S11C,D).

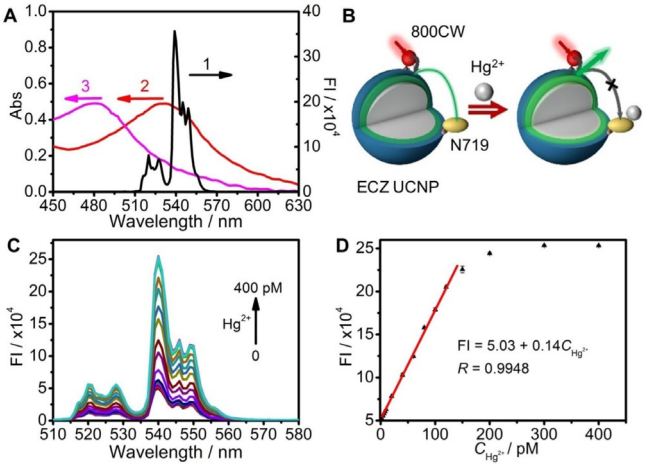

Figure 4. A) Luminescence spectrum of 0.03 mg mL^{-1} ECZ UCNPs under 808 nm excitation (10 W cm^{-2}) (1) and absorption spectra of N719 before (2) and after (3) reaction with Hg^{2+}. B) Schematic illustration of Hg^{2+} detection with ECZ UCNPs. C) Upconversion luminescence spectra of 0.03 mg mL^{-1} ECZ UCNP-N719 in response to Hg^{2+} at concentrations from 0 to 400 pM under 808 nm excitation (10 W cm^{-2}). D) Plot of emission peak intensity at 540 nm vs. Hg^{2+} concentration.

Photodynamic therapy (PDT), which uses light irradiation to produce ROS for cancer treatment,[19] was further performed to demonstrate the application of the designed mechanism. By conjugating a photosensitizer as the LRET acceptor on the surface, ECZ UCNPs could boost ROS generation (Figure 5A). Rose bengal (RB) with absorption at 470–600 nm (Figure S12A) was used as the photosensitizer. The synthesized ECZ UCNP-RB was further conjugated with folic acid-PEG2000-NHS to obtain ECZ UCNP-RB-FA for cell internalization, which increased the hydrodynamic diameter to 99 nm and decreased the zeta potential to +15.3 mV (Figure S12B). ECZ UCNP-RB-FA along with light irradiation possessed low cytotoxicity (Figure S12E,F). The ROS generation efficiency upon 808 nm irradiation was first determined in vitro by virtue of the ROS-sensing probe 1,3-diphenylisobenzofuran (DPBF). We observed 93.8% decrease of its absorbance peak at 412 nm within 3 min due to the fast consumption of DPBF by the abundant ROS generation. This was much greater than the 35% decrease reported for RB-loaded UCNP1@PEG/SiO_2,[20] and the 51.3% and 68.8% decrease we recorded for UCNP3@SiO_2-RB-FA and UCNP3@PEI-RB-FA, respectively, with 25 min irradiation at even much higher UCNP concentrations (Figure 5B,C). The intracellular ROS generation was examined with dihydroethidium (DHR), which shows emission at 510 nm under 488 nm light excitation upon ROS oxidation. The green emission was observed in Hela cells incubated with 50 μg mL^{-1} ECZ UCNPs-RB-FA after 808 nm irradiation (1.5 W cm^{-2}) for only 5 min (Figure 5D), indicating the high efficiency of the intracellular ROS generation. In contrast, much weaker green emission was observed for cells treated with UCNP3@PEI-RB-FA or UCNP3@SiO_2-RB-FA even after 25 min irradiation (Figure S12E,F). The dramatic en-

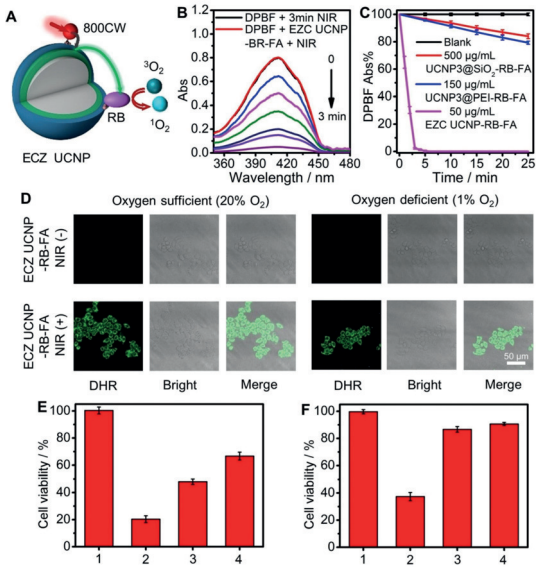

Figure 5. A) Schematic illustration of ROS generation with ECZ UCNP-RB. B) Absorbance of DPBF with NIR irradiation for 3 min and of DPBF in 50 μg mL^{-1} ECZ UCNP-RB-FA dispersion with NIR irradiation for 0 to 3 min. C) Decrease in DPBF absorbance in blank, 50 μg mL^{-1} ECZ UCNP-RB-FA, 150 μg mL^{-1} UCNP3@PEI-RB-FA, and 500 μg mL^{-1} UCNP3@SiO_2-RB-FA with NIR irradiation for different times. D) Confocal laser scanning microscopic images of HeLa cells after incubation with DHR for 30 min and then 50 μg mL^{-1} ECZ UCNPs-RB-FA under O_2-sufficient and O_2-deficient conditions for 6 h upon NIR irradiation for 5 min. E,F) MTT assays for HeLa cells as control (1) and HeLa cells incubated with 50 μg mL^{-1} ECZ UCNP-RB-FA (2), 150 μg mL^{-1} UCNP3@PEI-RB-FA (3), and 500 μg mL^{-1} UCNP3@SiO_2-RB-FA (4) under oxygen-sufficient (E) and -deficient (F) conditions.

hancement of ROS generation efficiency guarantees sufficient ROS production to overcome the limitations of PDT under hypoxic conditions.

To mimic the hypoxic environment, Hela cells were cultured in DMEM culture media under an O_2-deficient atmosphere[21] and transfected with ECZ UCNPs-RB-FA and DHR under an O_2-deficient atmosphere. The cells also showed strong DHR emission after 5 min irradiation (Figure 5D), indicating the efficient ROS generation by ECZ UCNP in a hypoxic microenvironment. The PDT efficiency of ECZ UCNP-RB-FA in O_2-sufficient and -deficient environments was verified with both an MTT assay and flow cytometric analysis. Upon PDT treatment, the cell viability became 20.3%, 40.8, and 66.7% under O_2-sufficient conditions and 37%, 86.7%, and 90.1% under O_2-deficient conditions for ECZ-UCNP-RB-FA, UCNP3@PEI-RB-FA, and UCNP3@SiO_2-RB-FA, respectively (Figure 5E,F). Flow cytometric analysis gave analogous results: apoptosis rates of 80.5%, 52.1%, and 33.5% in an O_2-sufficient environment and of 60.7%, 15.6%, and 11.8% in an O_2-deficient environment for ECZ-UCNP-RB-FA, UCNP3@PEI-RB-FA, and UCNP3@SiO_2-RB-FA, respectively (Figure S13). No doubt, ECZ UCNP-RB-FA shows an outstanding capability to overcome the key limitation of the hypoxic environment in PDT.

In conclusion, we propose a mechanism of efficient energy concentration with an energy-concentrating zone (ECZ) and an inert core to overcome the bottleneck of low energy transfer efficiency in UCNPs. The ECZ enhances light absorption using a new antenna 800CW linked with a bisphosphonate ligand, improves absorption energy transfer in an optimal energy absorption layer, and decreases energy migration distance. The ECS consists of an energy-emitting layer coated on the inert core that concentrates the upconversion energy to the emitting layer. The designed ECZ UCNPs decrease the depletion of absorption energy from the antenna to the UCNP and the upconversion energy from the emitting layer to the surface accepter. The energy concentration helps ECZ UCNPs to achieve 3600 times amplification in luminescence intensity and an energy transfer efficiency near 60% for outstanding LRET-based applications. Particularly, the boosted energy transfer efficiency and upconversion luminescence intensity provides a new avenue to address the key problem of the hypoxic environment in cancer PDT.

Acknowledgements

We gratefully acknowledge the National Natural Science Foundation of China (21635005, 21827812, 21890741, 21605083), National Research Foundation for Thousand Youth Talents Plan of China, Natural Science Foundation of Jiangsu Province (BK 20160644), State Key Laboratory of Analytical Chemistry for Life Science (5431ZZXM1806), Specially-appointed Professor Foundation of Jiangsu Province, and Program for Innovative Talents and Entrepreneurs of Jiangsu Province.

Conflict of interest

The authors declare no conflict of interest.

Keywords: nanoparticles · photodynamic therapy · upconversion nanoparticles

How to cite: *Angew. Chem. Int. Ed.* **2019**, *58*, 12117–12122
Angew. Chem. **2019**, *131*, 12245–12250

[1] a) N. Wu, L. Bao, L. Ding, H. Ju, *Angew. Chem. Int. Ed.* **2016**, *55*, 5220–5224; *Angew. Chem.* **2016**, *128*, 5306–5310; b) T. Liang, Z. Li, P. Wang, F. Zhao, J. Liu, Z. Liu, *J. Am. Chem. Soc.* **2018**, *140*, 14696–14703; c) Z. Li, H. Yuan, W. Yuan, Q. Su, F. Li, *Coord. Chem. Rev.* **2018**, *354*, 155–168.

[2] S. Wen, J. Zhou, K. Zheng, A. Bednarkiewicz, X. Liu, D. Jin, *Nat. Commun.* **2018**, *9*, 2415.

[3] a) L. L. Li, R. Zhang, L. Yin, K. Zheng, W. Qin, P. R. Selvin, Y. Lu, *Angew. Chem. Int. Ed.* **2012**, *51*, 6121–6125; *Angew. Chem.* **2012**, *124*, 6225–6229; b) Z. Li, S. Lv, Y. Wang, S. Chen, Z. Liu, *J. Am. Chem. Soc.* **2015**, *137*, 3421–3427.

[4] S. Han, R. Deng, X. Xie, X. Liu, *Angew. Chem. Int. Ed.* **2014**, *53*, 11702–11715; *Angew. Chem.* **2014**, *126*, 11892–11906.

[5] a) R. Deng, J. Wang, R. Chen, W. Huang, X. Liu, *J. Am. Chem. Soc.* **2016**, *138*, 15972–15979; b) R. Roy, S. Hohng, T. Ha, *Nat. Methods* **2008**, *5*, 507–516.

[6] a) E. M. Chan, E. S. Levy, B. E. Cohen, *Adv. Mater.* **2015**, *27*, 5753–5761; b) Y. Zhong, I. Rostami, Z. Wang, H. Dai, Z. Hu, *Adv. Mater.* **2015**, *27*, 6418–6422; c) J. Zuo, D. Sun, L. Tu, Y. Wu, Y. Cao, B. Xue, Y. Zhang, Y. Chang, X. Liu, X. Kong, W. J. Buma, E. J. Meijer, H. Zhang, *Angew. Chem. Int. Ed.* **2018**, *57*, 3054–3058; *Angew. Chem.* **2018**, *130*, 3108–3112; d) F. Wang, R. Deng, J. Wang, Q. Wang, Y. Han, H. Zhu, X. Chen, X. Liu, *Nat. Mater.* **2011**, *10*, 968–973.

[7] Y. Zhong, G. Tian, Z. Gu, Y. Yang, L. Gu, Y. Zhao, Y. Ma, J. Yao, *Adv. Mater.* **2014**, *26*, 2831–2837.

[8] F. Wang, J. Wang, X. Liu, *Angew. Chem. Int. Ed.* **2010**, *49*, 7456–7460; *Angew. Chem.* **2010**, *122*, 7618–7622.

[9] a) W. Zheng, S. Zhou, Z. Chen, P. Hu, Y. Liu, D. Tu, H. Zhu, R. Li, M. Huang, X. Chen, *Angew. Chem. Int. Ed.* **2013**, *52*, 6671–6676; *Angew. Chem.* **2013**, *125*, 6803–6808; b) D. J. Gargas, E. M. Chan, A. D. Ostrowski, S. Aloni, M. V. Altoe, E. S. Barnard, B. Sanii, J. J. Urban, D. J. Milliron, B. E. Cohen, P. J. Schuck, *Nat. Nanotechnol.* **2014**, *9*, 300–305.

[10] X. Chen, L. Jin, W. Kong, T. Sun, W. Zhang, X. Liu, J. Fan, S. F. Yu, F. Wang, *Nat. Commun.* **2016**, *7*, 10304.

[11] a) G. Chen, W. Shao, R. R. Valiev, T. Y. Ohulchanskyy, G. S. He, H. Ågren, P. N. Prasad, *Adv. Opt. Mater.* **2016**, *4*, 1760–1766; b) G. Chen, J. Damasco, H. Qiu, W. Shao, T. Y. Ohulchanskyy, R. R. Valiev, X. Wu, G. Han, Y. Wang, C. Yang, H. Agren, P. N. Prasad, *Nano Lett.* **2015**, *15*, 7400–7407; c) D. J. Garfield, N. J. Borys, S. M. Hamed, N. A. Torquato, C. A. Tajon, B. Tian, B. Shevitski, E. S. Barnard, Y. D. Suh, S. Aloni, J. B. Neaton, E. M. Chan, B. E. Cohen, P. J. Schuck, *Nat. Photonics* **2018**, *12*, 402–407; d) W. Zou, C. Visser, J. A. Maduro, M. S. Pshenichnikov, J. C. Hummelen, *Nat. Photonics* **2012**, *6*, 560–564; e) J. Xu, P. Yang, M. Sun, H. Bi, B. Liu, D. Yang, S. Gai, F. He, J. Lin, *ACS Nano* **2017**, *11*, 4133–4144; f) S. L. Lin, Z. R. Chen, C. A. Chang, *Nanotheranostics* **2018**, *2*, 243–257; g) X. Wu, Y. Zhang, K. Takle, O. Bilsel, Z. Li, H. Lee, Z. Zhang, D. Li, W. Fan, C. Duan, E. M. Chan, C. Lois, Y. Xiang, G. Han, *ACS Nano* **2016**, *10*, 1060–1066.

[12] a) C. Liu, L. Chang, H. Wang, J. Bai, W. Ren, Z. Li, *Anal. Chem.* **2014**, *86*, 6095–6102; b) S. Bhuckory, E. Hemmer, Y.-T. Wu, A. Yahia-Ammar, F. Vetrone, N. Hildebrandt, *Eur. J. Inorg. Chem.*

2017, 5186 – 5195; c) J. Liu, J. Cheng, Y. Zhang, *Biosens. Bioelectron.* **2013**, *43*, 252 – 256.
[13] D. Liu, X. Xu, Y. Du, X. Qin, Y. Zhang, C. Ma, S. Wen, W. Ren, E. M. Goldys, J. A. Piper, S. Dou, X. Liu, D. Jin, *Nat. Commun.* **2016**, *7*, 10254.
[14] W. Ren, S. Wen, S. A. Tawfik, Q. P. Su, G. Lin, L. A. Ju, M. J. Ford, H. Ghodke, A. M. van Oijen, D. Jin, *Chem. Sci.* **2018**, *9*, 4352 – 4358.
[15] W. Wei, G. Chen, A. Baev, G. S. He, W. Shao, J. Damasco, P. N. Prasad, *J. Am. Chem. Soc.* **2016**, *138*, 15130 – 15133.
[16] J. Wang, R. Deng, M. A. MacDonald, B. Chen, J. Yuan, F. Wang, D. Chi, T. S. Hor, P. Zhang, G. Liu, Y. Han, X. Liu, *Nat. Mater.* **2014**, *13*, 157 – 162.
[17] V. Muhr, C. Wurth, M. Kraft, M. Buchner, A. J. Baeumner, U. Resch-Genger, T. Hirsch, *Anal. Chem.* **2017**, *89*, 4868 – 4874.
[18] Q. Liu, J. Peng, L. Sun, F. Li, *ACS Nano* **2011**, *5*, 8040 – 8048.
[19] P. Agostinis, K. Berg, K. A. Cengel, T. H. Foster, A. W. Girotti, S. O. Gollnick, S. M. Hahn, M. R. Hamblin, A. Juzeniene, D. Kessel, M. Korbelik, J. Moan, P. Mroz, D. Nowis, J. Piette, B. C. Wilson, J. Golab, *CA-Cancer J. Clin.* **2011**, *61*, 250 – 281.
[20] F. Lu, L. Yang, Y. Ding, J.-J. Zhu, *Adv. Funct. Mater.* **2016**, *26*, 4778 – 4785.
[21] J. Kim, H. R. Cho, H. Jeon, D. Kim, C. Song, N. Lee, S. H. Choi, T. Hyeon, *J. Am. Chem. Soc.* **2017**, *139*, 10992 – 10995.

Manuscript received: May 22, 2019
Revised manuscript received: June 28, 2019
Accepted manuscript online: July 5, 2019
Version of record online: July 25, 2019

